Dielectric Behavior of Mechano-chemically Synthesized [(CH3NH3)3Bi2Br9]: A Lead Free Hybrid Perovskite

Swagatalaxmi Pujaru
Jadavpur University
Priyabrata Sadhukhan
Jadavpur University
Basudev Ghosh
Jadavpur University
Arup Dhara
Burdwan Raj College
Sachindranath Das (sachindas15@gmail.com)
Jadavpur University Faculty of Science https://orcid.org/0000-0002-6938-6701

Research Article

Keywords: Lead free hybrid perovskite, Dielectric properties, Rietveld refinement, Impedance spectroscopy

Posted Date: February 12th, 2021

DOI: https://doi.org/10.21203/rs.3.rs-218681/v1

Dielectric behavior of mechano-chemically synthesized $[(CH_3NH_3)_3Bi_2Br_9]$: A lead free hybrid perovskite.

Swagatalaxmi Pujaru[1,2], Priyabrata Sadhukhan[1], Basudev Ghosh[2], Arup Dhara[3], Sachindranath Das*[1]

[1]*Department of Instrumentation Science, Jadavpur University, Jadavpur, Kolkata-700032, India*
[2]*Department of Physics, Jadavpur University, Jadavpur, Kolkata-700032, India*
[3]*Department of Physics, Burdwan Raj College, Burdwan, WB-713104, India*

**Corresponding Author*
Dr. Sachindranath Das
E-mail: sachindran.das@jadavpuruniversity.in; *sachindas15@gmail.com*
Tel.: +91 3324572965

ABSTRACT:

Lead free hybrid halide perovskite $(CH_3NH_3)_3Bi_2Br_9$ has been successfully synthesized by mechano-chemical method. The microstructure analysis by Rietveld's refinement method revealed that the crystal belongs to trigonal system with space group $P\bar{3}m1$. The obtained microstructural parameters are well in agreement with the previously published data. Temperature-dependent ac conductivity, impedance spectroscopy, and complex dielectric properties have been investigated in detail. The negative temperature coefficient of resistance behaviour reveals the semiconducting nature of the materials. The complex impedance spectroscopy also supports the semiconducting nature of the sample with activation energy for conduction ~0.38 eV.

KEYWORDS: Lead free hybrid perovskite; Dielectric properties; Rietveld refinement; Impedance spectroscopy.

I. Introduction:

The most promising sources for sustainable and renewable clean energies are solar energy and wind energy. Solar energy is widely acceptable because of its availability and low maintenance cost. Silicon based solar cells are the main stake holders in the commercial market. However, its cost to power ratio is relatively high due to its high production cost. In this scenario, methylammonium lead halide based perovskites ($CH_3NH_3PbX_3$: X=I,Cl,Br) have inspired the research community for its remarkable opto-electronic and electrical properties like long carrier diffusion length, high optical absorption coefficient, ease of band gap engineering, good defect tolerance, low trap density, excellent photoluminescence efficiency [1-5]. But it exhibits some environmental issues due to use of highly toxic heavy material (lead) along with serious stability issue in moisture and UV irradiation [6]. It becomes a social responsibility for the researchers to find an alternative material in place of lead, without affecting the photo conversion efficiency of the semiconductor. Among different methylammonium lead halide perovskites, $CH_3NH_3PbBr_3$ is more stable against moisture and UV light for its cubic lattice structure [7–9]. $CH_3NH_3PbBr_3$ also shows better charge diffusion length than $CH_3NH_3PbI_3$ [10]. But its wide band gap (2.3 eV) does not allow to absorb light over 540 nm. Thus, only a small portion of the sunlight is absorbed and exhibit poor efficiency (~10%). To find out the alternatives, optoelectronic properties of hybrid perovskites with different inorganic and organic cations like Cs^+, $CHN_2H_4^+$ (or FA^+) for A-site; Bi^{2+}, Sn^{2+} for B-site have already been investigated [11-12]. Bi^{2+} may be a suitable replacement of Pb due its close position in the periodic table. But, most lead free organo-metalic hybrid perovskite shows less stability in presence of light, humidity and even in open environment. Moreover, slight variation in compositional elements can change the optoelectronic properties

drastically. Comparatively stable lead-free hybrid halide perovskite typically $(CH_3NH_3)_3Bi_2Br_9$ (MABB) may be a promising material for optoelectronic applications. The MA^+ cations (MA = CH_3NH_3) and inorganic $BiBr_6$ octahedra plays a crucial role in electrical and optoelectronic properties. Researchers explored that the materials have trigonal and monoclinic phase depending on applied pressure. But the detailed electrical properties are rare in literature. Hence the synthesis and detailed study of MABB is very important.

In this paper, we have investigated the structural properties by XRD analysis and electrical properties by impedance spectroscopy. Ball milling method has been employed to synthesize this material due to its easy control of experimental conditions. Moreover, it has been reported that the stability of some hybrid perovskites synthesized by ball milling method exhibit higher stability than the chemically synthesized material[13]. Here, we have reported how the real and imaginary part of impedance of the material changes with frequency and temperature. From imaginary part of impedance, relaxation frequency, relaxation time and activation energy of charge carriers have been calculated from Arrhenius plot ($\ln(\tau)$ vs 1000/T) and was found nearly identical with the calculated value from dc conductivity analysis. A detailed analysis on $Z'(\omega)$-$Z''(\omega)$ plot (Cole-Cole) was carried out to understand the grain, grain boundary and electrode material attribution to the ac transportation for all temperatures. A broad study on frequency dependent dielectric permittivity was carried out at different temperatures.

II. EXPERIMENTAL DETAILS:

A. Chemicals:

Methylamine Bromide [$CH_3NH_2Br_3$], Bismuth Bromide [$BiBr_3$, Sigma Aldrich, 99%], Dimethylformamide (DMF) [C_3H_7NO, Merck Chemicals, 99.5%] Toluene [Merck Chemicals]

were used for this experiment. All the chemicals were of analytical grade and used without any further purification.

B. Synthesis of $(CH_3NH_3)_3Bi_2Br_9$:

Methylammonium Bromide (MABr) was synthesized via a wet chemical route. Methylamine (60 ml) and Hydrobromic acid (25 ml) were mixed at 0 ^{0}C for 2 hours in an ice bath. The resulting solution was then heated at 60 ^{0}C for 3 hours. A white color solid was obtained and it was then washed several times with diethyl ether to remove the unreacted part. Further, it was dried at 60 ^{0}C for overnight to prepare powder MAB. Then, MABr and $BiBr_3$ powders were taken within a 100ml closed stainless steel milling jar along with stainless steel balls having the ball to powder mass ratio 40:1. Milling was performed in a planetary ball mill (Gaelon enterprise, China) for six hours at 500 RPM following a 5 min gap between two milling sessions of 5 min. In the milling process, toluene was used as a milling medium to avoid the unreacted part during the impact between balls, jars and materials. After six-hours of operation, the material was collected in colloidal form which was then dried in vacuum at 50 ^{0}C to evaporate the milling medium. Thus, the synthesized material was obtained in the powder form and used for XRD and electrical measurements.

III. Result and Discussion:

A. XRD and Structural analysis

The synthesized powder MABB obtained by ball-milling of AX_3 and BiX_3 (A= CH_3NH_2, X= Br) was analyzed by X-ray diffraction (XRD) pattern with Rietveld's refinement. The XRD pattern has several peaks, which confirms the crystalline nature of the synthesized material. The XRD peaks do not match with the peak of the constituent materials which confirms the formation of

new material after milling. XRD pattern of the mechanochemically-synthesized powder has been shown in Fig.1(a). The XRD peaks are in good agreement with the published Inorganic Crystal Structure Database (ICSD) [14]. We have generated the CIF for the simulation process of the XRD pattern using Rietveld's refinement method. The Rietveld software MAUD permits simultaneous and refinement of both structural and microstructure parameters through Marquardt least-squares method for reduction of the difference between the simulated/calculated (I_c) and observed (I_o) intensities. The irrelevant residue of fitting ($I_C - I_O$) between experimental/observed (I_O) and simulated/calculated (I_C) intensities is plotted under the XRD pattern, which indicates the good quality of fitting. The Caglioti parameters U, V, and W, (Caglioti et al., 1958) instrumental asymmetry and Gaussianity parameters were obtained for instrumental corrections using a Si standard and kept fixed during refinements. The analysis revealed that the crystal belongs to the trigonal system of space group $P\bar{3}m1$. The best refined cell parameters obtained by Rietveld refinement are *a= 8.218(9) Å, b= 8.218(9) Å and c= 10.008(7) Å.* The obtained values of the cell parameters are very close to the previously published work[15]. The estimated values of the crystallite size and microstrain from this refinement are ~103 nm and 6.6 x 10^{-4} respectively.

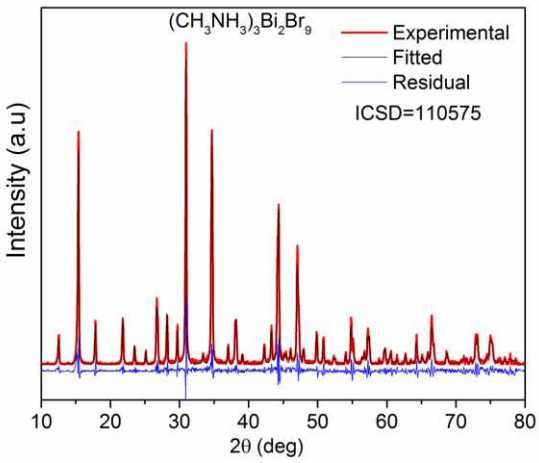

Fig.1: (a) Typical output of XRD patterns of Rietveld analysis for MABB: Red, black and blue lines represent experimental (I_o), simulated (I_c) and residual ($I_o - I_c$) patterns, respectively.

B. Impedance analysis:

The electrical characteristics of MABB plate was investigated using the complex impedance [Z* = Z'(ω) - iZ''(ω)] spectroscopy technique in the frequency range 4 Hz to 1 MHz and temperature range 333 K to 453 K. This technique is principally suitable to determine electrical conductivity and carrier relaxation. The frequency dependent representation of real part (Z'(ω)) of complex impedance Z* = Z'(ω) - iZ''(ω) in temperature range 333 K - 453 K for $[(CH_3NH_3)_3Bi_2Br_9$ has been shown in Fig.2(a). At low frequency region, value of Z ′ (ω) is high and the value decreases with the increase of frequency for all temperatures. It shows high value at low temperature and decreases with the increase of temperature for the frequency range 4Hz-1MHz. This indicates that the temperature coefficient of resistance (NTCR) is negative and the material is semiconductor. Due to lowering of trapped charge density and increase in mobility of charge carriers with increase in temperature decreases the value of Z′. The combined effect of dipolar, electronic and orientation polarization generally attribute this type of behaviour.[16] At higher frequency, the graphs tend to merge. This insignificant variation has been observed in Z'(ω) with temperature at higher frequency indicating the presence of space charge. It suggests greater value of ac conductivity for higher temperature in high frequency domain due to modified barrier properties and release of space charge.[17]

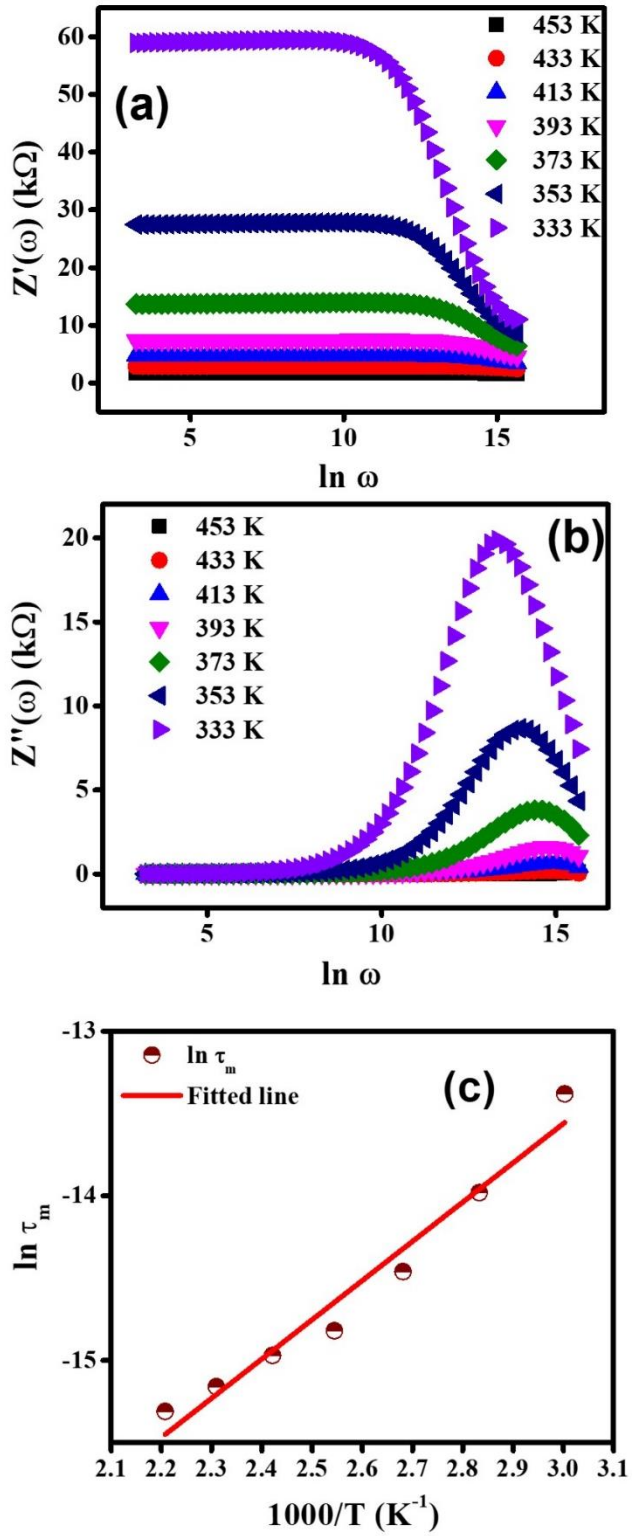

Fig.2: (a)Real part of impedance (Z') vs frequency, (b) Imaginary part of impedance (Z'') vs frequency, (c) Arrhenius plot for calculation of activation energy (E_a).

Fig.2(b) Shows the frequency dependent imaginary part Z"(ω) of impedance for frequency range 4 Hz-1 MHz. The entire curve associated a peak at high frequency region, conventionally known as "Relaxation peak". In these characteristics, peak position (relaxation frequency) has shifted towards the high frequency as well as reduction in the height are also observed with the increase in temperature. This implies the thermally activated electrical response of charge carrier within the material. The broadening of the peak and consequent shift of peak position along with the asymmetric distribution suggest that there are different electrical phenomena simultaneously occurring in the material involving a distribution of relaxation times. Variation of relaxation frequency with temperature implies that temperature has an impact on relaxation process, and mean relaxation time is not constant over whole temperature range. Temperature dependence of the mean relaxation time mainly assigns the contribution of localized relaxation[18]. The broad relaxation peak implies the distribution of relaxation time over a frequency range indicating non-Debye type dielectric relaxation. [19] Normally, Relaxation time (τ_p) is defined as time lapse between applied field and polarization in the material which can be determined using the equation $\omega_p\tau_p = 1$, where ω_p ($=2\pi f_p$) denote relaxation frequency. In this analysis, relaxation frequency has been accounted corresponding to the peak position in $Z''(\omega)$ vs $\ln\omega$ plot at different temperatures, hence, τ_p has been calculated using equation $\omega_p\tau_p = 1$. Variation of relaxation time with temperature follows Arrhenius relation $\tau_p = \tau_0 exp\left(\frac{-E_a}{kT}\right)$, where τ_o, E_a, K and T represents pre-exponential factor, activation energy, Boltzmann constant and absolute temperature, respectively. Fig.2(c) shows the $\ln\tau_p$ vs 1000/T plot and the activation energy (E_a) has been calculated as 0.25 eV from the linearly fitted curve. The moderate value of E_a suggests that some relaxation species (e.g. defect) definitely present in conduction process and also

confirmed the contribution of ionic conduction as well as possible hopping of ions [$(CH_3NH_3)^+$, Bi^{2+} Br^-] are responsible for the relaxation.

The complex impedance plot (Cole-Cole plot) i.e. Z'(ω) vs Z''(ω) with different temperature has been shown in Fig.3, where, Z'(ω) and Z''(ω) contain the resistive and capacitive part of complex impedance, respectively. It is a fact that if the relaxation mechanism deviates from ideal Debye type relaxation, the Cole-Cole plot does not always yield a perfect and symmetric semicircular arc. Here, one depressed semicircular arc has appeared with center below the real axis which implies relaxation process follow non-Debye type relaxation and it may be due to the bulk effect.[21] The single semicircle appreciates overall contribution of grain and grain boundary to the capacitive and resistive part of complex impedance also. It is evident from the figure that radius of these semicircular arc decreases with the increase of temperature. Such type of characteristics clearly reveals charge transportation process is thermally activated and confirms semiconducting behavior of the material within the entire temperature range. Correlation between ac electrical properties and microstructure of material was investigated by equivalent circuit. An equivalent circuit has been obtained using two parallel resistance-capacitor (RC) element connect in series. As the semicircular part due to grain and grain boundary are quite overlapping, it is very difficult to find out the contribution of grain and grain boundary separately. The Cole-Cole [Z'(ω)-Z''(ω)] plot was fitted by EC Lab program and computed value of R_g, C_g, R_{gb} and C_{gb} has shown in table-1. At lower and high frequency, grain boundary and grain have a significant contribution to the impedance value, respectively. No other relaxation process, such as sample-electrode interface effects, could be observed through this formalism in the applied frequency and temperature range. The radii of the semicircles decrease with increasing temperatures, indicating the semiconducting behavior of the material. It is evident from the table 1 that grain boundary of

$(CH_3NH_3)_3Bi_2Br_9$ offered higher resistance compared to grain. The junction barriers are sufficient to trap the charge carriers and desirably grain and grain boundary resistance decrease with rising temperature. The value of grain boundary capacitance (c_{gb}) decreases with decrease of temperature.

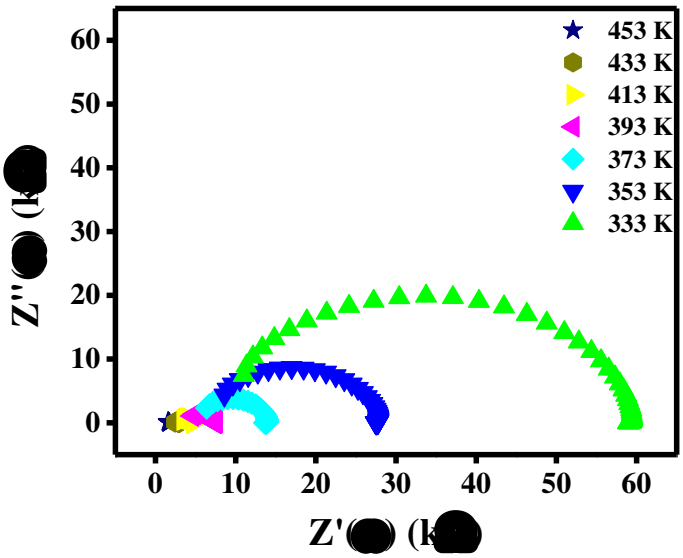

Fig.3 Cole-Cole plots of MABB at different temperatures

Table 1. Variation of different equivalent circuit parameters of MABB at elevated temperatures

Temperature (℃)	R_{gb} (kΩ)	R_g (kΩ)	C_g (pF)	C_{gb} (pF)
60	52.096	7.543	29.86	2.83
80	21.926	6.257	40.14	1.48
100	8.779	5.243	64.28	1.92
120	4.016	3.536	0.000113	0.085
140	2.444	2.247	0.000116	0.006
160	1.814	1.081	0.000190	0.004

So, c_{gb} depends on barrier layer width (d) and d maintains by trapped charge carriers at the junctions. With increase in temperature, layer width becomes quite small as a result c_{gb} becomes very small. Indeed, due to the fact grain boundary capacitance decreases with increase in temperature proportional to the ratio of trapped charge carriers to free carrier density.[22] From the total resistance value ($R= R_g+R_{gb}$), the dc conductivity of the samples has been calculated at different temperatures using the relation σ_{dc} = D/RA, where 'D' and 'A' are the thickness and cross-sectional area (1.33 cm^2) of the pellet, respectively.

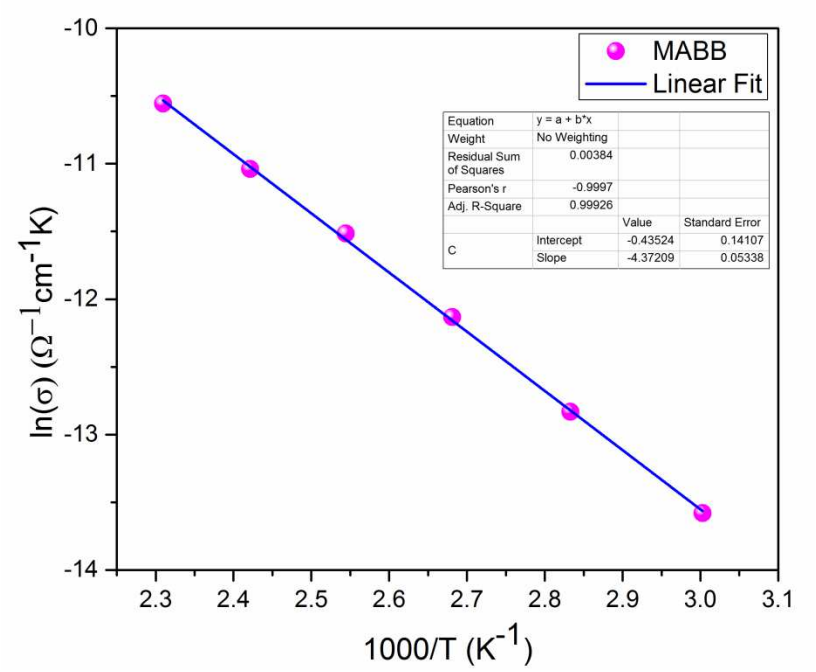

Fig.4 Arrhenius plot [(lnσ(T) vs 1000/T] of MABB.

The activation energy (E_a) for conduction has been estimated from the Arrhenius plot (Fig.4) using the relation

$$\ln\sigma_{dc}(T) = \ln\sigma_0 - \frac{E_a}{KT} \quad (2)$$

where T, K and σ_0 are the absolute temperature, Boltzmann constant and the pre-exponential parameter, respectively. The estimated value of the activation energy of the sample is found to be 0.38 eV and the value of the pre-exponential factor σ_0 is 0.6471 $\Omega^{-1}cm^{-1}$. The obtained value of activation energy is in well agreement with the value obtained from figure 2(c).

C. Dielectric properties and conductivity:

A material reflects its dielectric properties when an external field is applied to this material. Fig.5 shows the variations of dielectric constant ($\varepsilon' \; and \; \varepsilon''$) with respect to the applied frequency at different temperature of the surrounding environment of MABB. The value of ε' showed an increasing tendency in the temperature range from 333 K to 453 K. It is clear from the Fig.5 that the material follows the external field up to ~ 300 Hz (resonance frequency of the material), after that the dielectric constant become independent of the applied frequency at all measured temperature. Both real and imaginary part of dielectric constants decreased exponentially with increasing frequency at each temperature. The higher value of dielectric constants at low frequency region might be due to the interfacial space charge formation. The values at very low frequency increased significantly as temperature increased, due to the enhanced thermally activated free carriers. The possible reason behind the trend is based on Maxwell-Wagner polarization mechanism. In this mechanism, at the frequency higher than the resonance frequency, less space charge is accumulated at the grain boundary region and consequently minimizes the dielectric losses.

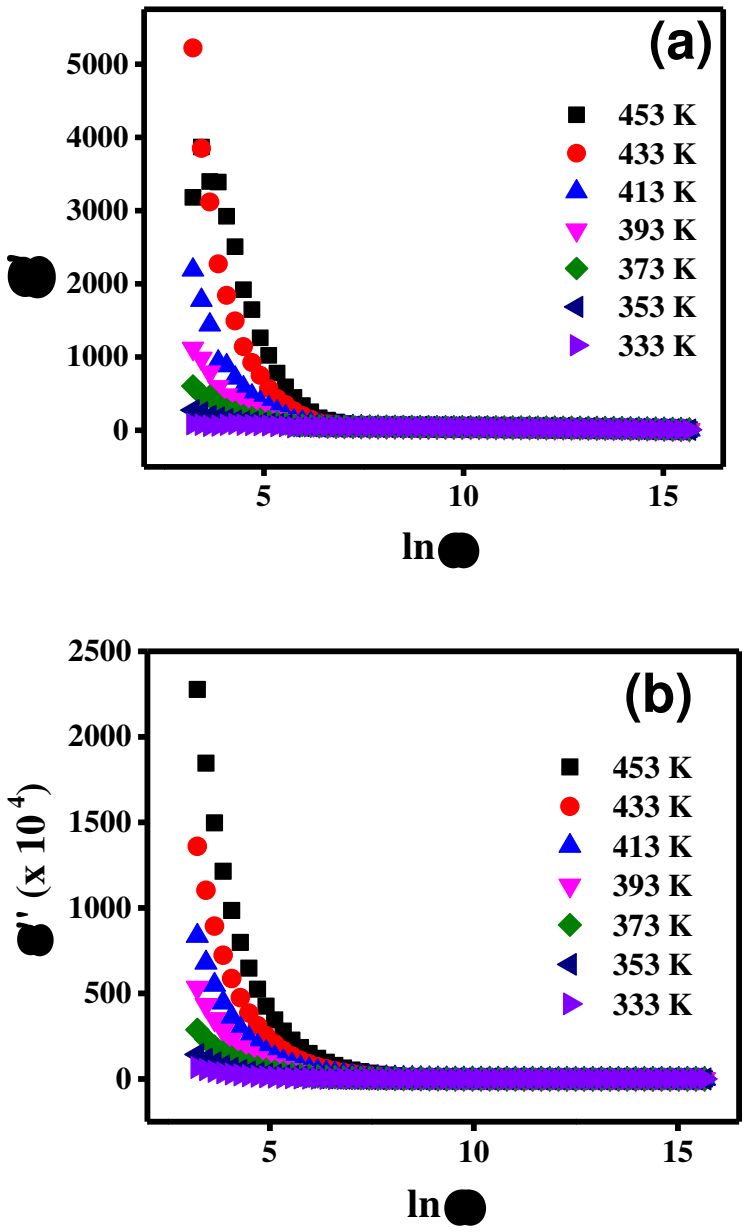

Fig.5 Log frequency variation of (a) real part (ε') of complex dielectric constant (ε^*) of MABB at different temperatures.

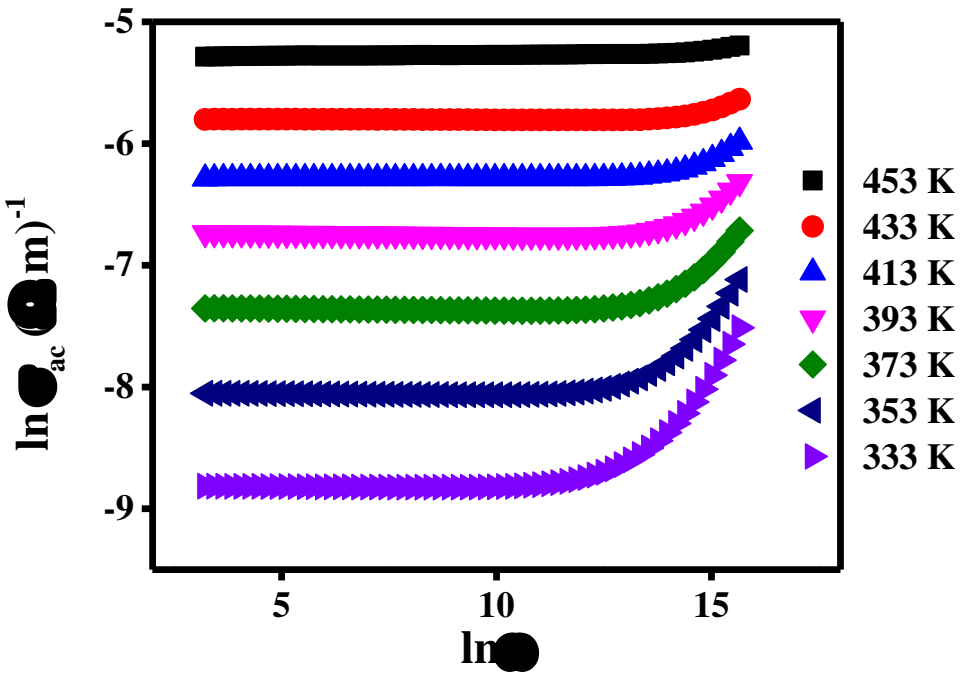

Fig.6 Log frequency variation of (ln σ) of MABB at different temperatures.

D. **Electrical conductivity:**

The AC electrical conductivity has been calculated using the relation $\sigma_{ac} = \omega\varepsilon'\varepsilon_0 tan\delta$ where ε_0 is free space permittivity, ε' is the real part of dielectric constant, ω is frequency and $tan\delta$ is the loss tangent[11]. Figure 6 represent the variation of electrical conductivity with frequency in log scale. At low frequency region, at a particular temperature, the electrical conductivity is frequency independent and the value increases as the temperature increase which is attributed to the DC conductivity of semiconducting materials. It is also evident from the figure that as the temperature increases, frequency independent plateau type region extended towards higher frequency region. At low frequency, the electric field could not perturb the hopping mechanism and the long-range mobilization of charge carriers are responsible for such plateau region. This

effect is more dominant at higher temperature. This behavior reflects the semiconducting nature of MABB. Transportation of charge carriers between different localized states increases with frequency which results in the increase of ac conductivity at high frequency[11,24]. Actually, positive charge cloud [$(CH_3NH_3)^+$, Bi^{2+}] is surrounding by closely packed negatively charged bromide ions within the material but two charge centers can be treated as isolated from each other. The interaction of localized charge carrier with such a slightly deformed polar material gives rise to form polaron which are moving in between nearest neighbor sites, known as polaron hopping. Further increase of frequency, available localized charge for conduction increases due to the fact that occupancy of trap center reduces with frequency. As a result of which conductivity increases by enhancing the electrons and holes hopping in the form of polaron[12,25].

IV. Conclusions

In the present study, lead free hybrid halide perovskite $(CH_3NH_3)_3Bi_2Br_9$ has been synthesized by mechano-chemical technique. Microstructural, temperature and frequency dependent electrical properties have been studied extensively. The microstructure analysis by Rietveld's refinement method revealed that the material belongs to trigonal system of space group $P\bar{3}m1$ which matches well with existing data. The impedance spectroscopy reveals the contribution from grain and grain boundary in the total resistance of the sample. The relaxation process strongly depends on temperature. The complex impedance spectroscopy supports the semiconducting nature of the sample with activation energy for conduction 0.38 eV. Thus, the detailed studies on impedance spectroscopy, relaxation behavior, AC conductivity, activation

energy of this lead-free hybrid perovskite material will explore the possibilities to use this material for optoelectronic applications.

V. ACKNOWLEDGEMENT:

Sachindranath Das is thankful to Department of Science and Technology and Bio- Technology, Government of West Bengal [247(Sanc.)/ST/P/S&T/16G-36/2017 dated 25/03/2018] for research funding.

VI. REFERENCES:

(1) M. M. Lee, J. Teuscher, T. Miyasaka, T. N. Murakami, H.J. Snaith; *Science 338;* 643–647 (**2012).**
(2) P. Sadhukhan, S. Kundu, A. Roy, A. Ray, P. Maji, S. K. Pradhan and S. N. Das; *Crystal Growth & Designs; 18*, 3428-3432 **(2018)**.
(3) N. J. Jeon, J. H. Noh, W. S. Yang, Y. C. Kim, S. Ryu, J. Seo, S.I. Seok; *Nature 517;* 476–480 (**2015).**
(4) P. Sadhukhan, S.N. Das; *Solar Energy, 194*, 563–568 **(2019).**
(5) P. Sadhukhan, A. Pradhan, S. Mukherjee, P. Sengupta, A.Roy, S. Bhunia, S.N. Das; *Appl. Phys. Lett. 114*,131102 **(2019).**
(6) A. Kojima, K. Teshima, Y. Shirai, T. Miyasaka; *J. Am. Chem. Soc. 131 (17),* 6050–6051 **(2009).**
(7) W. Zhu, C. Bao, F. Li, T. Yu, H. Gao, Y. Yi, J. Yang, G. Fu, X. Zhou, Z. Zou; *Nano Energy 19,* 17–26 **(2016).**
(8) J.H. Noh, S.H. Im, J.H. Heo, T.N. Mandal, S.I. Seok; *Nano Lett. 13 (4),* 1764–1769 **(2013).**
(9) R. Sheng, A. Ho-Baillie, S. Huang, S. Chen, X. Wen, X. Hao, M. A. Green; *J. Phys. Chem. C 119 (7),* 3545–3549. **(2015),**
(10) S. Aharon, B. Cohen, L. Etgar; *J. Phys. Chem. C 118 (30),* 17160–17165 **(2014).**
(11) P. Maji, S. Chatterjee, S. N. Das; *Ceramics International 45,* 6012-6020 **(2019)**
(12) P. Maji, A. Ray, P. Sadhukhan, S. Chatterjee, S. N. Das; *Journal of Applied Physics 124*, 124102 **(2018)**
(13) C A López, M C Alvarez-Galván, M V Martínez-Huerta, F Fauth, J A Alonso; *CrystEngComm ,22,* 767 **(2020)**
(14) M. M Yao, C. H. Jiang, J. S. Yao, K. H. Wang, C. Chen, Y. C. Yin, B. S. Zhu, T. Chen, H. B. Yao; *Inorg. Chem.; 58*, 11807–11818 **(2019).**
(15) Q. Li, L. Yin, Z. Chen, K. Deng, S. Luo, B. Zou, Z. Wang, J. Tang, Z.Quan; *Inorg. Chem. 58*, 1621–1626 **(2019)**
(16) S. Pujaru, P. Maji, P. Sadhukhan, A. Ray, B. Ghosh, S.N. Das; *Journal of Materials Science: Materials in Electronics; 31*, 8670–8679 **(2020).**

(17) S. Das and A. Ghosh, *J. Phys. Chem. B 121*, 5422 **(2017).**
(18) C. Tealdi, G. Chiodelli, L. Malavasi, G. Flor, C. Fisica, I. Unita, V. Taramelli, I. Pavia, *J. Mater. Chem 14*, 3553 **(2004).**
(19) T. Paul and A. Ghosh, *J. Appl. Phys. 121*, 135106 **(2017).**
(20) M.S. Sheikh, A.P. Sakhya, A. Dutta, and T.P. Sinha, *Thin Solid Films 638*, 277 **(2017).**
(21) M.S. Sheikh, A.P. Sakhya, P. Sadhukhan, A. Dutta, S. Das, and T.P. Sinha, *Ferroelectrics 514*, 146 **(2017).**
(22) Z. Li, M. Yang, J.S. Park, S.H. Wei, J.J. Berry, and K. Zhu, *Chem. Mater. 28*, 284 **(2016).**
(23) A. Dhara, S. Sain, S. Das, and S.K. Pradhan, *Mater. Res. Bull. 97*, 169 **(2018).**
(24) X.Z. Zuo, J. Yang, B. Yuan, D.P. Song, X.W. Tang, K.J. Zhang, X.B. Zhu, W.H. Song, J.M. Dai, and Y.P. Sun, *J. Appl. Phys. 117*, 0 **(2015).**
(25) N.H. Vasoya, P.K. Jha, K.G. Saija, S.N. Dolia, K.B. Zankat, and K.B. Modi, *J. Electron. Mater. 45*, 917 (**2016**).

Figures

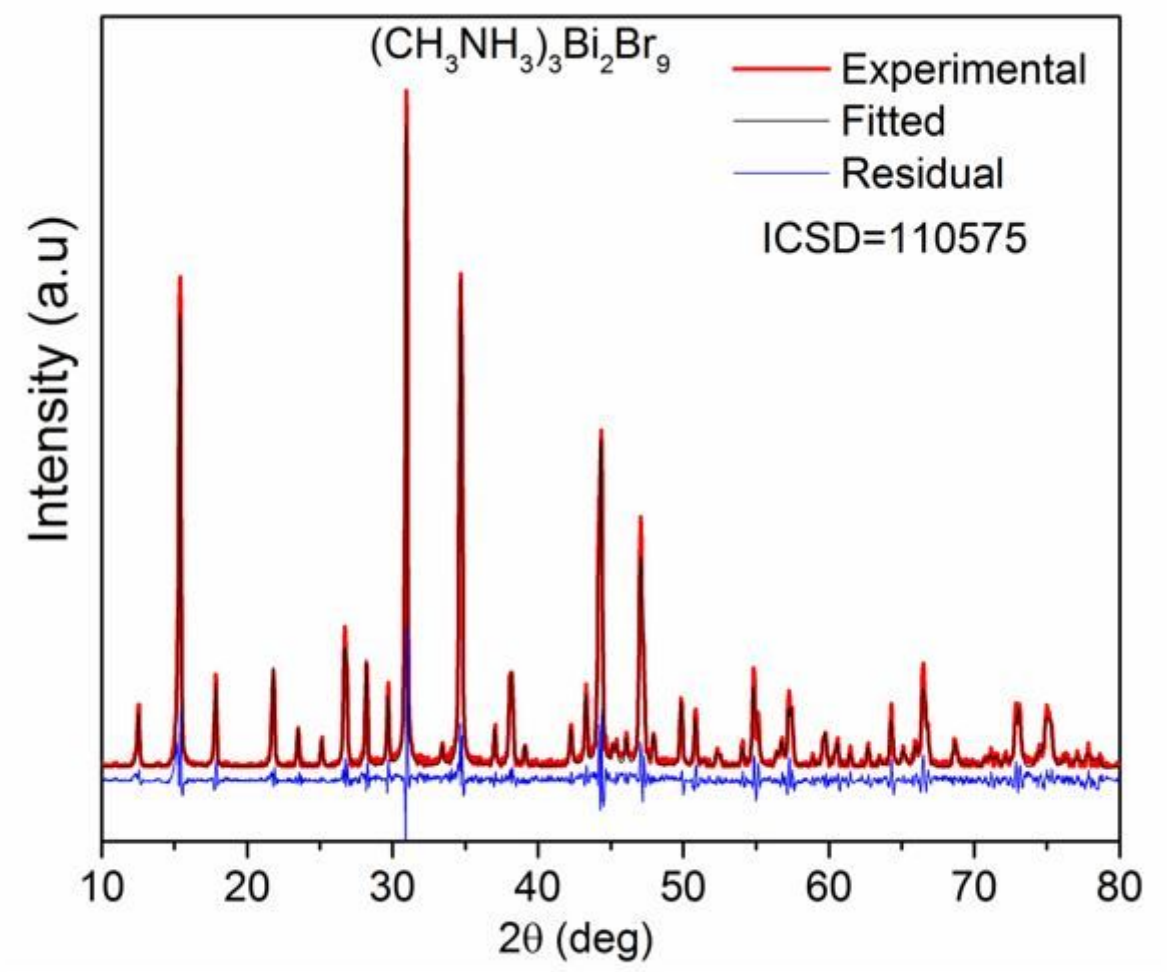

Figure 1

(a) Typical output of XRD patterns of Rietveld analysis for MABB: Red, black and blue lines represent experimental (Io), simulated (Ic) and residual (Io−Ic) patterns, respectively.

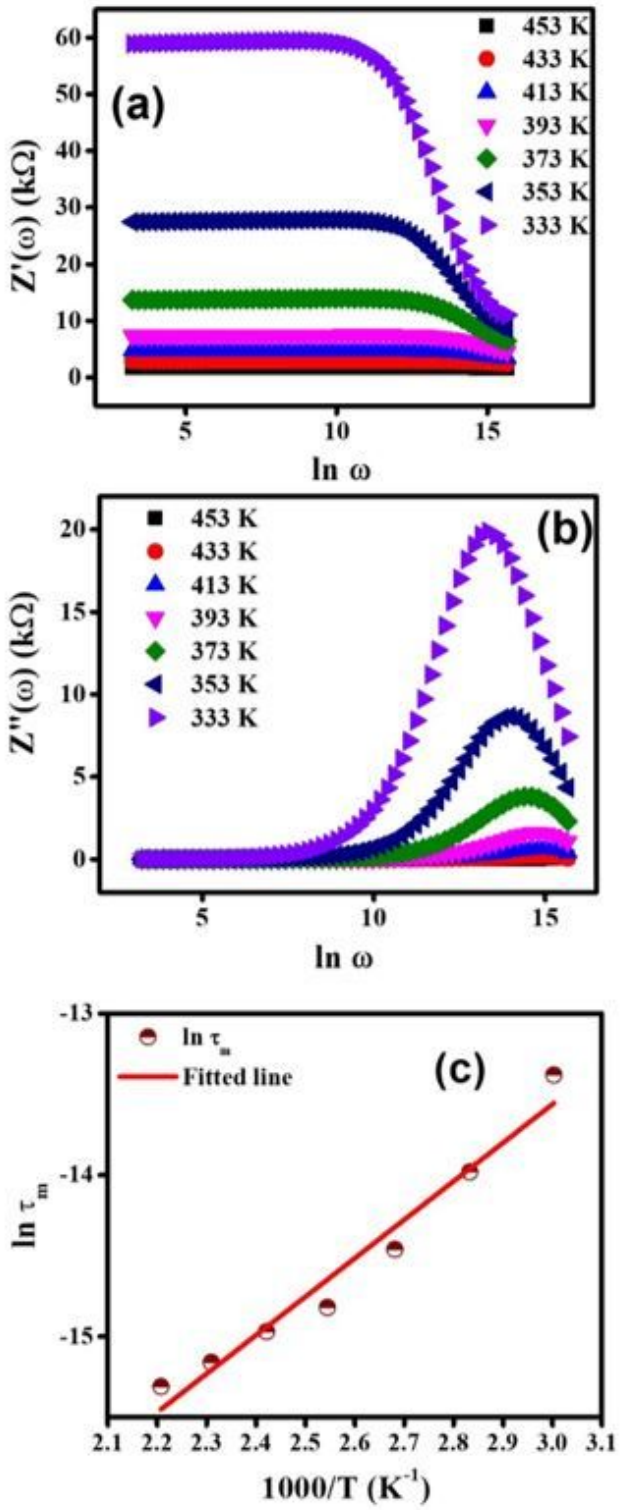

Figure 2

(a)Real part of impedance (Z′) vs frequency, (b) Imaginary part of impedance (Z″) vs frequency, (c) Arrhenius plot for calculation of activation energy (Ea).

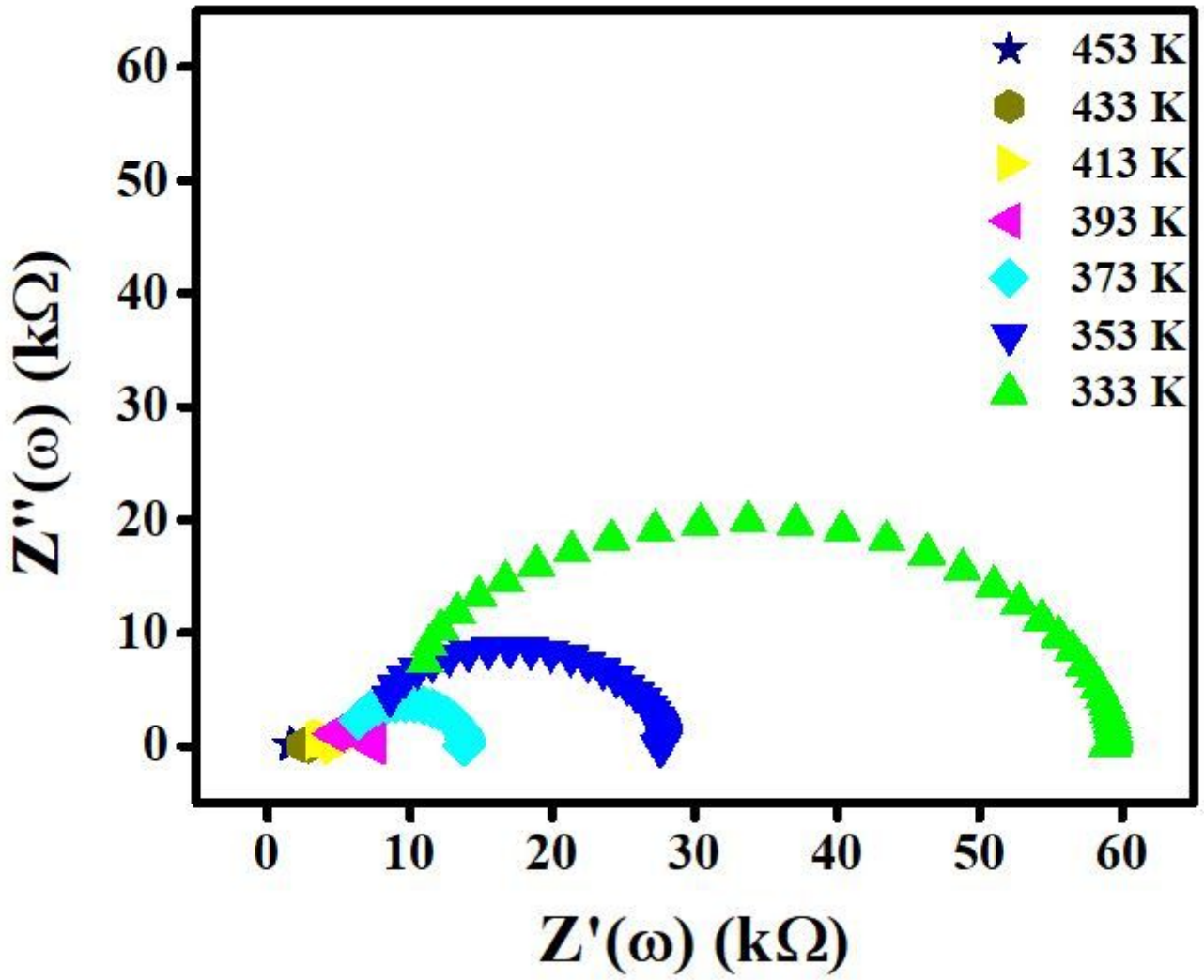

Figure 3

Cole-Cole plots of MABB at different temperatures

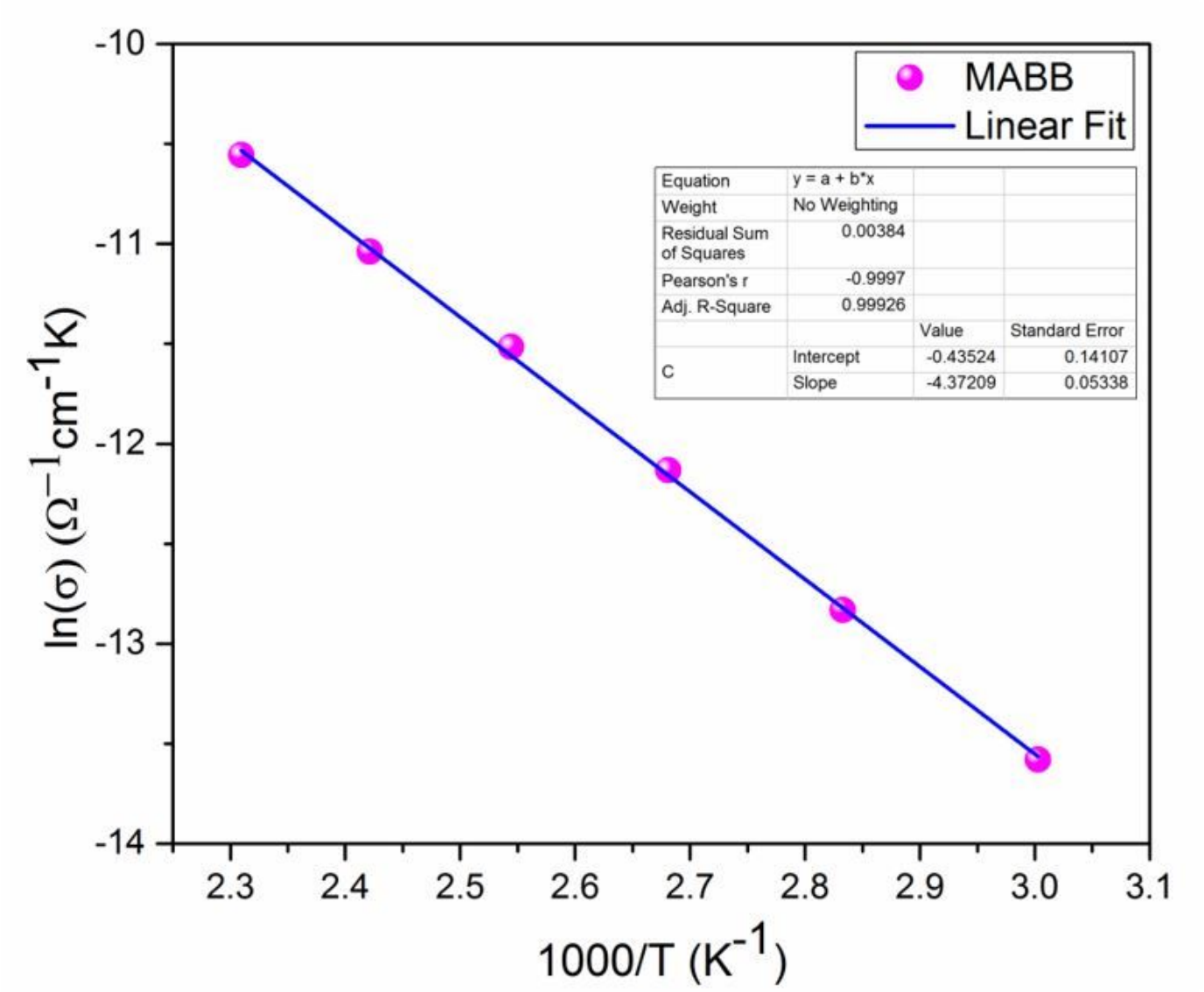

Figure 4

Arrhenius plot [(lnσ(T) vs 1000/T] of MABB.

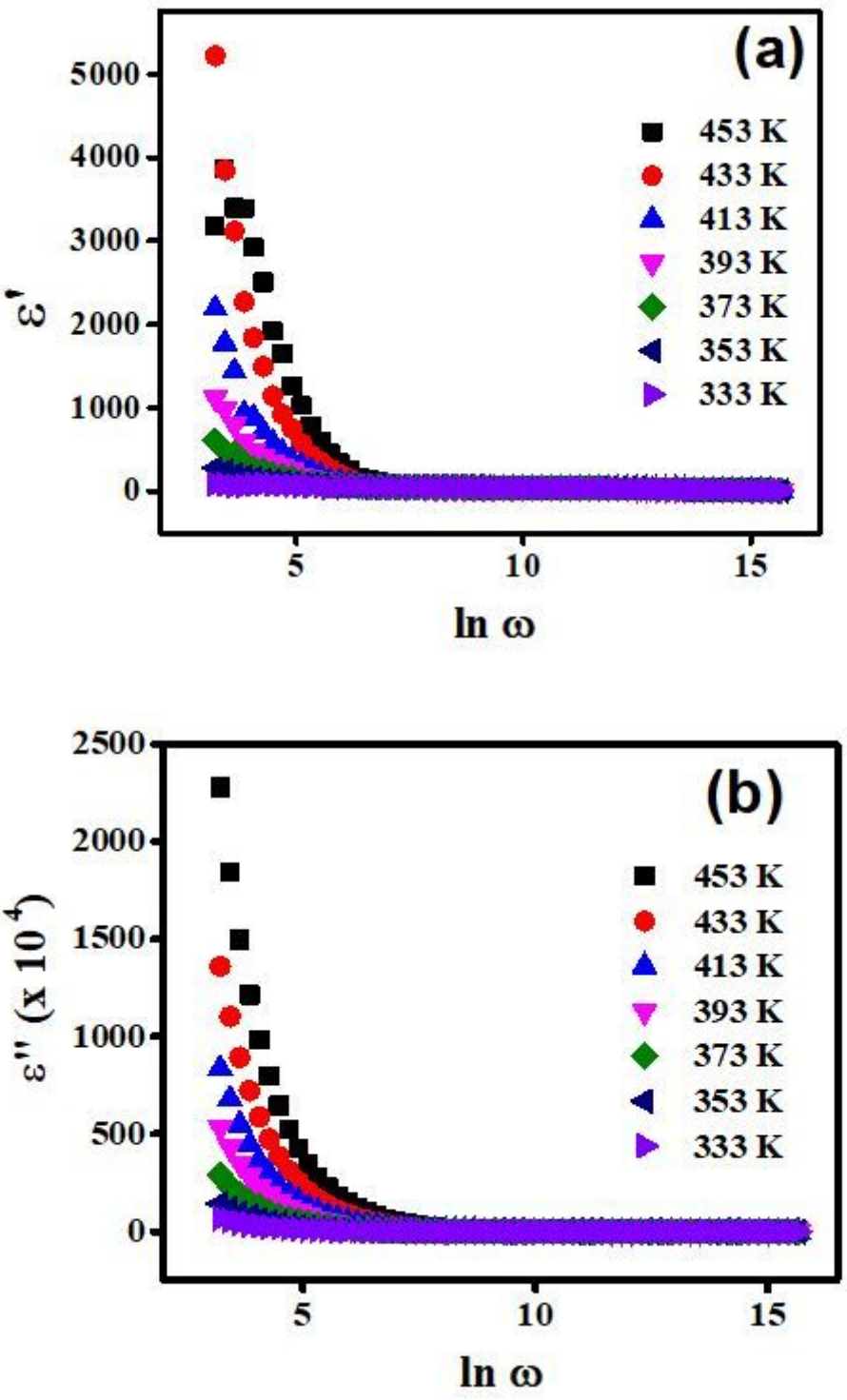

Figure 5

Log frequency variation of (a) real part (ε^') of complex dielectric constant (ε^*) of MABB at different temperatures.

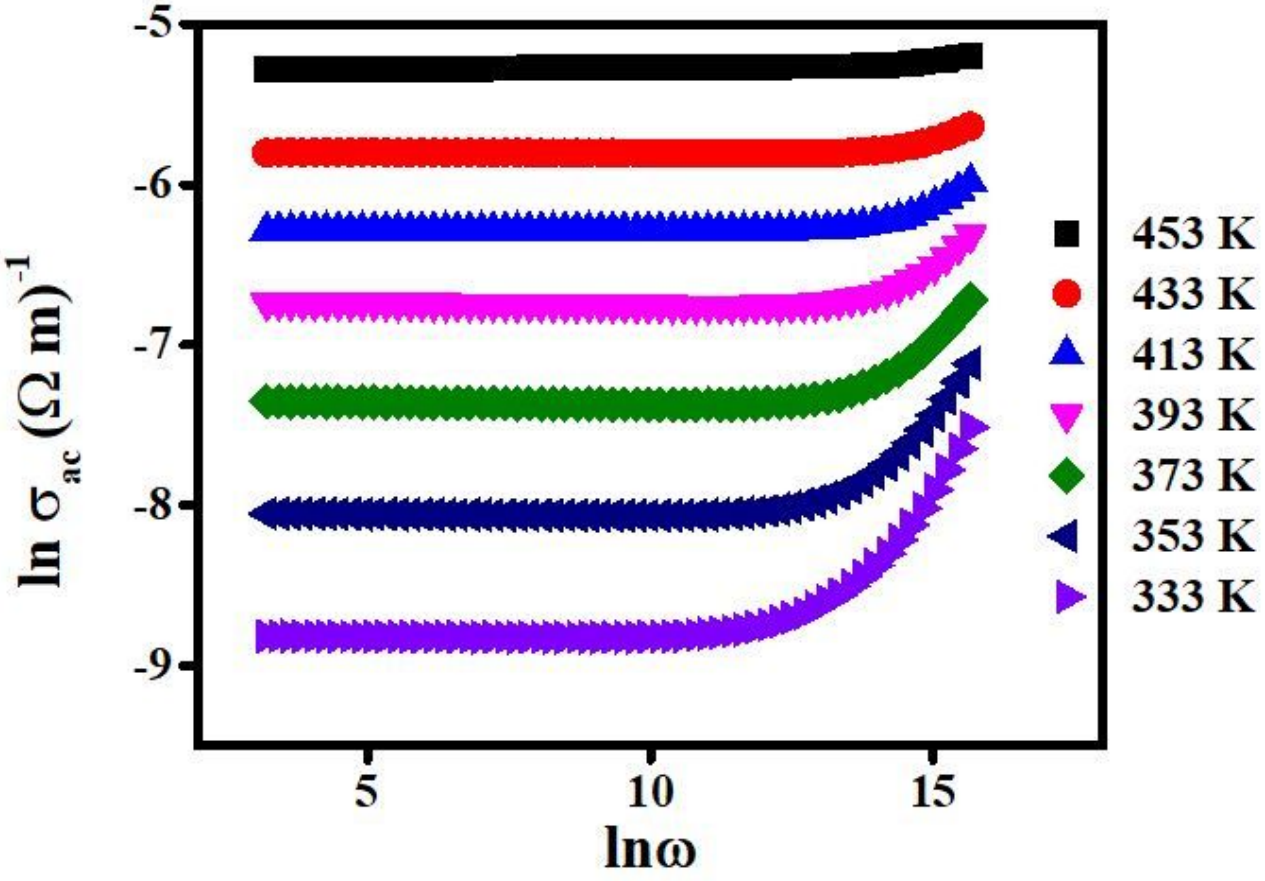

Figure 6

Log frequency variation of (ln σ) of MABB at different temperatures.